Journal of Materials Chemistry A

ROYAL SOCIETY OF CHEMISTRY

PAPER

View Article Online
View Journal | View Issue

Check for updates

Cite this: *J. Mater. Chem. A*, 2026, **14**, 3955

Molecular origin of negative lithium transference in electrolytes with star-shaped multivalent anions

Chao Fang, *[a] Ian Woosley,[b] Saheli Chakraborty,[bc] David M. Halat, [d] Nitash P. Balsara *[bc] and Rui Wang *[bc]

Large multivalent anions have gained increasing attention for their potential to improve lithium transference in electrolytes. We employ large-scale molecular dynamics simulations based on the Onsager transport framework to investigate ion transport in a lithium electrolyte with star-shaped multivalent anions. The simulations show that t_+^0, the cation transference number with respect to solvent velocity, is negative over a wide range of concentration. This is consistent with experimental data reported previously. The simulation-based Onsager transport coefficients reveal that the magnitudes of the cation–cation, anion–anion, and cation–anion correlations are comparable, a signature of highly correlated motion in the electrolyte. Examination of the cation solvation environment indicates the presence of strong cation–anion association across the entire concentration range, which leads to negative t_+^0 on the order of -1. Both simulation and experiment also show that the maximum value of t_+^0 reaches 0 when the cation concentration is $c_+ = 0.4$ M. This is the concentration at which the anions begin to spatially overlap, and lithium ions serve as dynamic linkers to balance cation–cation and cation–anion correlations. Our results provide molecular-level insights into the origin of transference in multivalent electrolytes.

Received 16th July 2025
Accepted 13th December 2025

DOI: 10.1039/d5ta05739f

rsc.li/materials-a

[a]*Thrust of Sustainable Energy and Environment, The Hong Kong University of Science and Technology (Guangzhou), Guangzhou, Guangdong 511453, China. E-mail: chaofang@hkust-gz.edu.cn*

[b]*Department of Chemical and Biomolecular Engineering, University of California, Berkeley, California 94720, USA. E-mail: ruiwang325@berkeley.edu; nbalsara@berkeley.edu*

[c]*Materials Sciences Division, Lawrence Berkeley National Laboratory, Berkeley, California 94720, USA*

[d]*Department of Chemistry, Colorado School of Mines, Golden, Colorado 80401, USA*

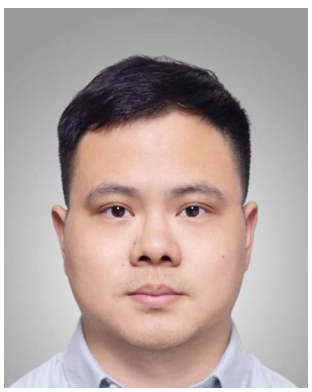

Chao Fang

Dr Chao Fang has been an Assistant Professor in Sustainable Energy and Environment Thrust at HKUST(GZ) since 2024. He obtained a B.S. in Theoretical and Applied Mechanics from University of Science and Technology of China in 2015 and a PhD in Mechanical Engineering from Virginia Tech in 2019, followed by postdoctoral research at UC Berkeley and Lawrence Berkeley National Laboratory. His research focuses on the molecular-level simulation of transport phenomena in soft matters such as polymer and gel electrolytes. His work has been published as first/corresponding author in journals such as Nat. Mater., Sci. Adv., PRL, JACS Au, and Chem. Sci.

Introduction

The performance of rechargeable lithium batteries relies on the selective transport of working cations.[2–4] In electrolytes consisting of a binary salt and solvent, continuum ion transport can be predicted when three ion transport properties are given: the conductivity (κ), the salt diffusion coefficient (D), and the cation transference number with respect to the solvent motion (t_+^0).[3,5,6] Unlike κ and D, which describe the collective motion of both ion species, t_+^0 quantifies the rate of cation transport relative to that of the anion and solvent.[5] The target value for t_+^0 is unity; in this case most of the energy used to charge the battery is to move the cations from the cathode to the anode.[4,5,7,8]

One approach to increase lithium transference is through the use of bulky anions as their substantial size suppresses anion mobility in accordance with the Stokes–Einstein relationship. While the distribution of charge in the anions is important, it is, perhaps, not surprising that commonly used anions in lithium electrolytes such as hexafluorophosphate (PF_6^-) and bis(trifluoromethanesulfonyl)imide ($TFSI^-$) are large. Bulky multivalent anions may, in principle, enable both high cation concentration and low anion mobility.[9–12] However, experimental and theoretical studies of solutions of linear polymeric anions and lithium counterions indicated that although the anion motion is slowed down, anion–anion correlations are enhanced through polymer backbone.[13–15] The

cation–anion correlations are also pronounced due to the formation of transient ionic aggregates.

Grafting of anions onto polyhedral oligomeric silsesquioxane (POSS), a promising battery electrolyte additive, to form multivalent macroions has recently gained attention in the context of lithium electrolytes.[16–18] In systems featuring POSS particles functionalized with bulky anion groups, *e.g.*, POSS-$(BF_3)_3$ and POSS-$(NSO_2CF_3)_8$, lithium transference numbers measured *via* the electrochemical method proposed by Bruce and Vincent[19] and Watanabe *et al.*[20] were reported to exceed 0.5.[21–23] In this method, the electrolyte is placed in a lithium–electrolyte–lithium symmetric cell, and the ratio of the final to initial current is taken to be the transference number. This method only gives the transference number in the limit of infinite dilution, and we therefore proposed using the term current fraction, ρ_+.[24] The reported ρ_+ values were higher than those derived from pulsed-field-gradient NMR (PFG-NMR) $t_{+,\mathrm{PFG\text{-}NMR}}$, which relies exclusively on ion self-diffusion coefficients. This discrepancy was attributed to the weak Li^+-POSS anion association.[23] In a subsequent study by Nguyen *et al.*, POSS particles grafted with 7–20 $TFSI^-$ anions (with remaining sites functionalized by oligomeric poly(-ethylene glycol)) were dispersed in tetraglyme solvents.[12] Electrochemical measurements again yielded high ρ_+ values in the range of 0.71–0.86.

More recently, lithium transference numbers were systematically measured in an electrolyte containing POSS-based macroions dissolved in a mixture of ethylene carbonate (EC) and dimethyl carbonate (DMC).[1] Each POSS particle has 8 PEG side chains and each side chain carries 2–3 $TFSI^-$ anions, which leads to a total valency of −20 per macroion. The measured ρ_+ values were large and much higher than $t_{+,\mathrm{PFG\text{-}NMR}}$. Crucially, however, a more accurate electrophoretic NMR (eNMR) measurement[25] revealed that the rigorously-defined cation transference number with respect to the solvent velocity, t_+^0, was negative across all salt concentrations. This finding together with those observed in polyanion electrolytes[15] demonstrates that merely slowing anion motion cannot guarantee an improvement in cation transference. These results highlight the critical role of complex correlations between cations, anions, and solvents that govern t_+^0. Insights into the origin of large negative t_+^0 not only clarify the limitations of the specific POSS-based electrolyte but also serve as a crucial basis for the rational development of other high-performance electrolytes. Herein, in this work, we investigate the molecular origin of low cation transference in POSS-based polyanionic electrolytes using molecular dynamics (MD) simulations. The continuum ion transport is quantified by employing the Onsager transport framework[6,14,26,27] that captures correlated motion between all species in the electrolyte. The simulation results are validated by experimental data. Insights into the continuum transport are obtained by examining species correlations, microscopic ion solvation, and the dynamics of ion association. The molecular-level understanding of ion transport in POSS electrolytes represents a vital diagnostic step that informs future electrolyte design strategies.

MD simulation methods

Our MD simulation system is set up to match the experimental condition reported in previous work.[1] The simulation system consists of POSS-PSLiTFSI salt (POSS nanoparticles containing lithium salt of polystyrene-4-sulfonyl(trifluoromethane sulfonyl) imide) and mixtures of EC and DMC solvents with equal weight. The POSS-based polyanion bears a valence of $z_- = -20$ as shown in Scheme 1a, which is the same as that used in previous experiments.[1] The simulation covers a Li^+ concentration range of 0.1 M to 0.8 M. The simulation box size is about 7.9 nm for $c_+ \geq 0.2$ M and 9.8 nm for $c_+ = 0.1$ M, respectively. The POSS core is modeled by 8 coarse-grained beads with force field parameters provided in previous literature,[28] whereas the side chains are treated with all-atom models, as shown in Scheme 1b. The side chains, solvent molecules, and Li^+ are modeled based on the OPLS-AA (optimized potentials for liquid simulations with all atom model) force fields.[29,30] The partial atomic charges for side chains and solvent molecules are fitted using the RESP method[31,32] *via* the Gaussian package[33] and Antechamber package.[34]

Equilibrium *NpT* simulations were conducted at 303 K and 1 bar using the Gromacs package (version 2022).[35] The temperature and pressure of the system were maintained *via* a velocity-rescaling thermostat[36] (time constant 1 ps) and Berendsen barostat[37] (time constant 1 ps), respectively. The bonds of the side chains and organic molecules are constrained using the LINCS algorithm.[38] Non-bonded interactions were calculated with the cut-off scheme (cutoff length 1.2 nm) Lennard-Jones potentials, while long-range electrostatics were handled *via* the particle mesh Ewald (PME) method.[39] Prior to equilibrium simulations, the system is first packed, and energy minimized. To ensure proper mixing, it then undergoes three cycles of 1 ns equilibration with temperature ramping between 303 K and 400 K. This is followed by another equilibrium simulation at target conditions (303 K and 1 bar) for 6 ns. Finally, an equilibrium simulation at 303 K and 1 bar is performed for 100 ns. At each salt concentration, four independent simulations are performed to enable sampling of the Onsager transport coefficients. The trajectories were saved with a frequency of 10 ps.

We employ the Onsager approach[14,26,27] to quantify the correlated motion of ions and solvents *via* simulation. The dynamic correlations between species i and j are captured by the transport coefficients L_{ij}^r:

$$L_{ij}^r = \frac{V}{6k_\mathrm{B}T}\lim_{t\to\infty}\frac{d}{dt}\left\langle \frac{1}{n_i}\sum_\alpha \Delta r_{i,\alpha}^r(t)\cdot\frac{1}{n_j}\sum_\beta \Delta r_{j,\beta}^r(t)\right\rangle \quad (1)$$

where the superscript r denotes the reference frame (either the solvent reference frame 0 or center-of-reference frame m), and i and j represent cation or anion. V, $k_\mathrm{B}T$, and n_i are respectively the system volume, thermal energy, and the particle number of species i. $\Delta r_{i,\alpha}^r(t)$ is the position of αth particle in species i relative to the solvent species (including EC and DMC, $r = 0$) or center-of-mass of the system ($r = m$). The definition of transport coefficients in eqn (1) is based on the form originally derived in the solvent reference frame.[26] Our analysis of dynamic

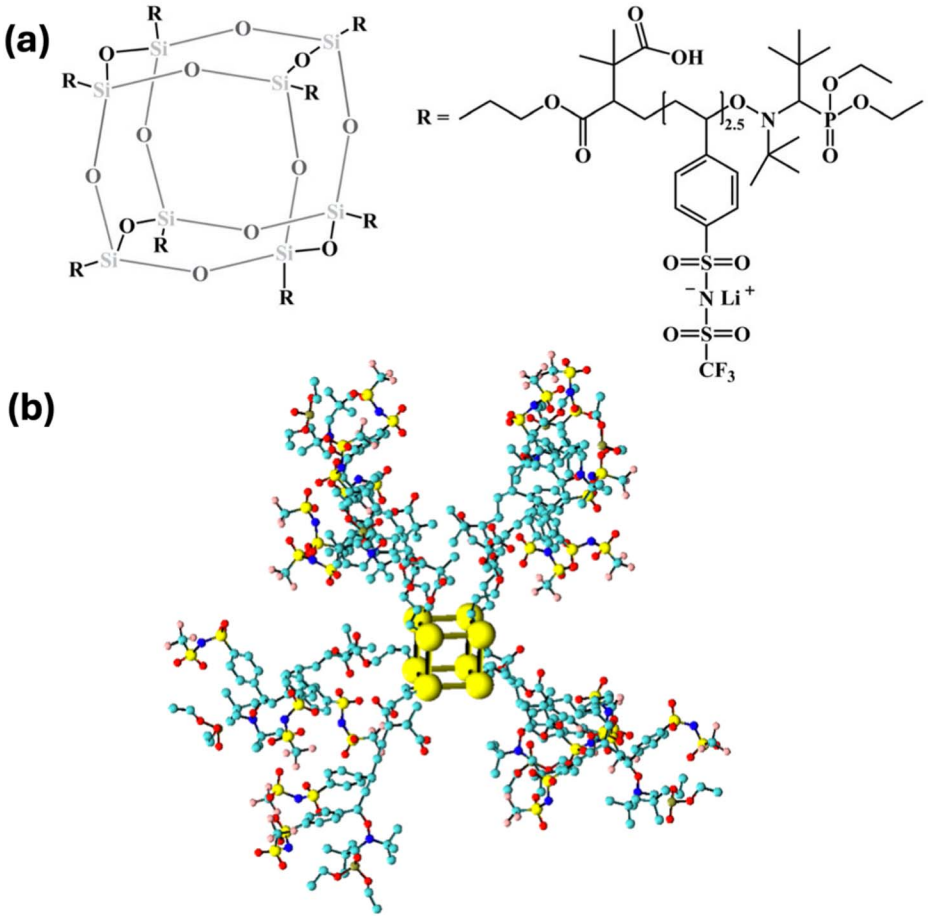

Scheme 1 (a) Illustration of the chemical structure of the POSS-based electrolyte, which is the same as that used in ref. 1. (b) Atomistic representation of the POSS-based anion. The coarse-grained beads of POSS core are shown in large yellow spheres. The side chains are shown in ball-and-stick model with carbon in cyan, nitrogen in blue, oxygen in red, fluorine in purple, phosphorus in olive, and sulfur in yellow. Hydrogen atoms are not shown for clarity.

correlations accounts for both reference frames. Previous work confirmed that they are consistent,[27,40–42] and the two sets of transport coefficients can be mapped onto each other.[40] The transport coefficients are fitted in the time regime spanning one order of magnitude, where the mean square displacement term $\mathrm{MSD}_{ij}^{r}(t) = \left\langle \frac{1}{n_i}\sum_{\alpha}\Delta r_{i,\alpha}^{r}(t)\cdot\frac{1}{n_j}\sum_{\beta}\Delta r_{j,\beta}^{r}(t)\right\rangle$ in eqn (1) follows a linear scaling with time. The maximum deviation of the scaling exponent γ ($\mathrm{MSD}_{ij}^{r}(t) \propto t^{\gamma}$) from unity is about 10% (see Table S1 in the SI).

Macroscopic transport properties, conductivity and transference numbers, were evaluated as functions of L_{ij}^{0}:

$$\kappa = F^2 c_+^2 z_+^2 (L_{++}^0 - 2L_{+-}^0 + L_{--}^0) \quad (2)$$

$$t_+^0 = \frac{L_{++}^0 - L_{+-}^0}{L_{++}^0 - 2L_{+-}^0 + L_{--}^0} \quad (3)$$

where F is the Faraday constant, and c_+ and z_+ are respectively the molar concentration and valence of Li^+. In multivalent system, the simplified forms in eqn (2) and (3) arise from the equality $c_+^2 z_+^2 = c_-^2 z_-^2$. The current fraction expression, originally derived for monovalent electrolytes in our previous work, is of the same form in multivalent systems:[43]

$$\rho_+ = \frac{1}{1+\mathrm{Ne}}, \quad \text{where} \quad \mathrm{Ne} = \frac{\left(L_{--}^0 - L_{+-}^0\right)^2}{L_{++}^0 L_{--}^0 - L_{+-}^0 L_{+-}^0}. \quad (4)$$

We refer to Ne as the Newman number.[44] One may also define the PFG-NMR-derived cation transference number based on self-diffusion coefficients of the ions:

$$t_{+,\mathrm{PFG}} = \frac{D_+}{D_+ - z_- D_-} \quad (5)$$

where D_+ and D_- are the simulations-based self-diffusion coefficients of the cation and anion, respectively. This measure of cation transference can be compared directly with that obtained experimentally using PFG-NMR.

Results and discussions

Correlated motion and ion transport

The atomistic model is first examined by comparing simulated self-diffusion coefficients with PFG-NMR measurements. Fig. 1a

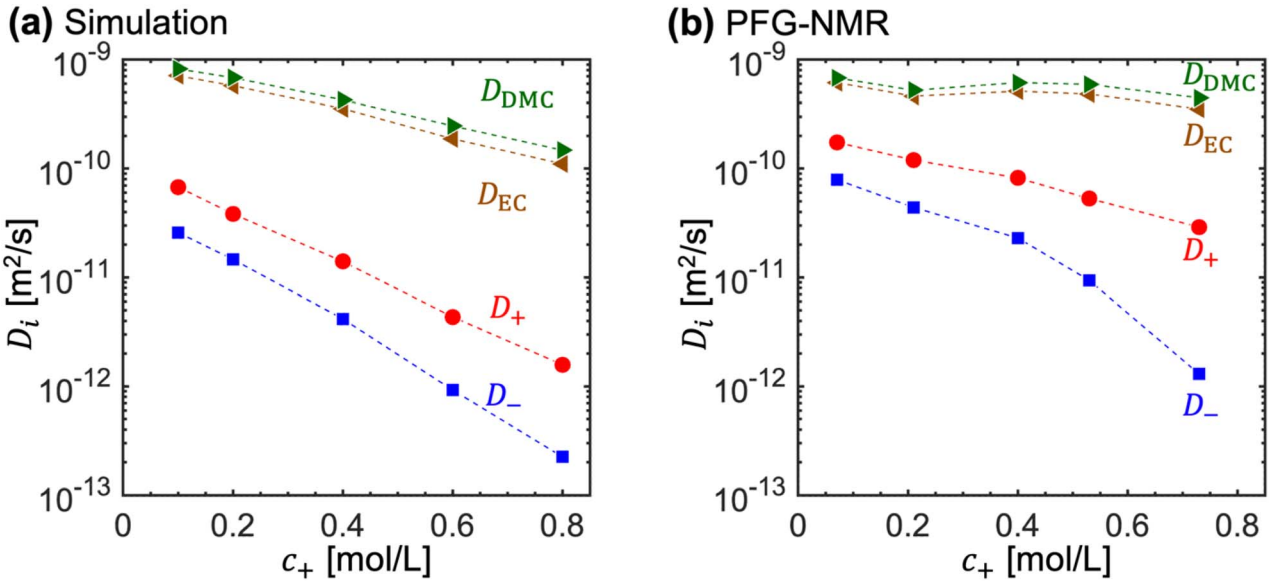

Fig. 1 Comparison of self-diffusion coefficients between (a) simulation and (b) experiment as a function of Li^+ molar concentration c_+. The PFG-NMR data in (b) are reproduced from ref. 1.

shows the diffusion coefficients of the cation (D_+), anion (D_-), and the solvents (D_{DMC} and D_{EC}) as a function of the molar Li^+ concentration, c_+, obtained from simulations. Fig. 1b shows the same quantities measured experimentally.[1] The simulations qualitatively capture important concentration dependence of the self-diffusivities for both charged ions and non-charged solvent species. The simulations show that D_{DMC} is slightly higher than D_{EC} at all salt concentrations. The ion mobilities are also much lower than those of solvents. Furthermore, D_+ is substantially higher than D_-, with this difference becoming more pronounced at higher salt concentrations. All these predictions are in good agreement with the results measured by experiments.

We also note that some quantitative discrepancies exist between simulation and experiment. The solvent and ion diffusivities predicted by MD simulations show stronger reduction as salt concentration increases in comparison with the experimental results. In addition, the simulated solvent diffusivities are marginally overestimated at low salt concentration but become underestimated as the concentration increases. These discrepancies can be explained by the charge polarization effects, which are not fully captured by the force field used in our MD simulations. The fixed-charge model involved in the simulation tends to overestimate the magnitude of the interactions between charged species.[45–47] This results in stronger cation–anion pairing in the simulations, which thus reduces ion mobility. The stronger cation–solvent interactions also cause greater suppression of solvent diffusion at high salt concentrations. Nonetheless, the MD simulations capture the important trends in the relative mobilities of ions and solvent molecules. We also evaluated standard correction approaches, including the use of an elevated temperature (323 K) and rescaling of ionic partial charges (by a factor of 0.8), at both low and high salt concentrations. Simulations conducted at a uniformly elevated temperature, however, resulted in a cation-to-anion diffusion coefficient ratio that is smaller than the experimentally measured values at high salt concentrations (see Fig. S2 and S3 in the SI). Additionally, simple charge rescaling led to a pronounced overestimation of cation mobility relative to anion as compared to experiments. These results indicate that while such corrections can improve the dynamics of the electrolyte, they do not transfer effectively to the present highly correlated, multivalent anion system without systematic reparameterization. Therefore, the original force field proves more suitable for our system. Although it may not capture the absolute dynamics with quantitative precision, it reproduces the relative cation–anion dynamics, the most critical factor in modeling the cation transference.

The transport coefficients defined by eqn (1) characterize the correlated motion of ions relative to a reference velocity. Fig. 2 depicts the concentration dependence of three transport coefficients in both the center-of-mass reference frame (L_{ij}^m) and solvent reference frame (L_{ij}^0). All transport coefficients reach a maximum value at a salt concentration of $c_+ = 0.2$ M. This maximum arises because of two competing effects. First, the transport coefficients rise with increasing c_+ at low concentrations due to an increase in the concentration of charge carriers. However, frictional interactions, which slow down transport, also increase exponentially with salt concentration, and the decrease of the Onsager coefficients at concentrations $c_+ > 0.2$ M signifies the regime wherein frictional effects are dominant. A comparison of the three Onsager coefficients reveals that anion–anion correlations (L_{--}^r) are the strongest at all concentrations. This observation suggests that a complete understanding of the behaviors of the cation transference requires properly accounting for correlations involving anions, a point we will discuss later. However, the magnitudes of all three coefficients are comparable in both reference frames, which

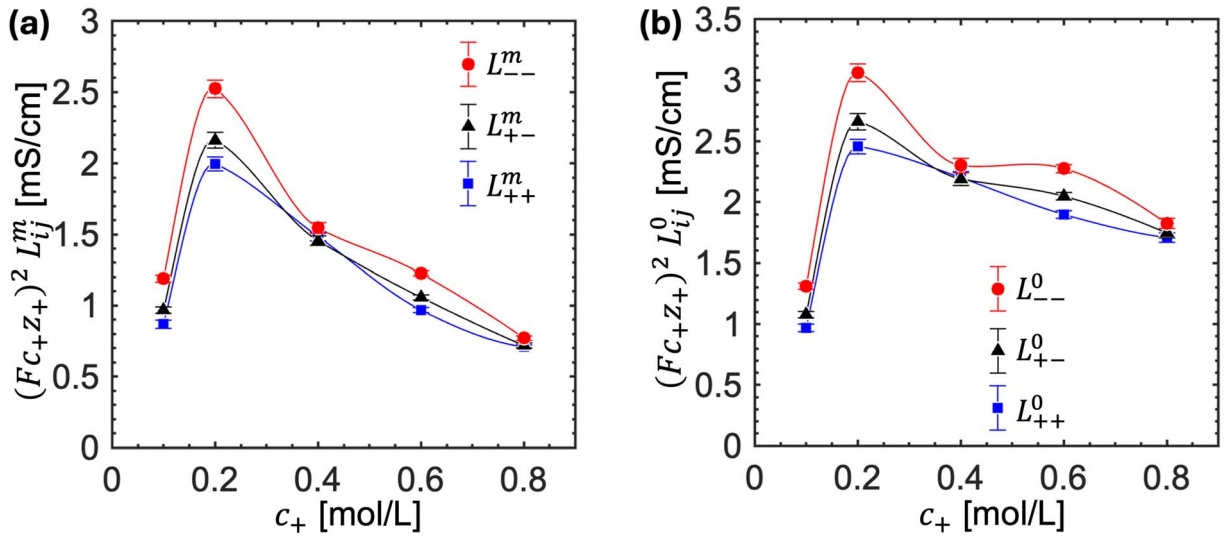

Fig. 2 Correlated motions of cations and anions as a function of salt concentration. Onsager transport coefficients that characterize cation–cation (L^r_{++}), anion–anion (L^r_{--}), and cation–anion (L^r_{+-}) correlated motions in (a) center-of-mass reference frame and (b) solvent reference frame.

indicates highly correlated motion of all charged species. As a result, the conductivities calculated by eqn (2) are about an order of magnitude smaller than transport coefficients (See Fig. S6 in the SI). Furthermore, it is interesting to note that the relative trends of the three transport coefficients are not affected by the choice of reference frame. This is in contrast to traditional lithium electrolytes containing univalent anions with strong cation–solvent interactions, *e.g.*, LiTFSI, where the choice of reference frame can reverse the sign of L^r_{+-}.[27,40] The resulting transference numbers in the solvent and mass reference frames only show a minor difference at all salt concentrations (Fig. S5 in SI).

Cation transference, as reflected by $t_{+,\mathrm{PFG}}$, ρ_+, and t^0_+, are calculated from the simulated Onsager transport coefficients using eqn (3)–(5). Fig. 3 compares the simulation results with experimental measurements. Both simulation and experiment values of the cation transference number estimated based on self-diffusion coefficients, $t_{+,\mathrm{PFG}}$, remain near 0.1 at low

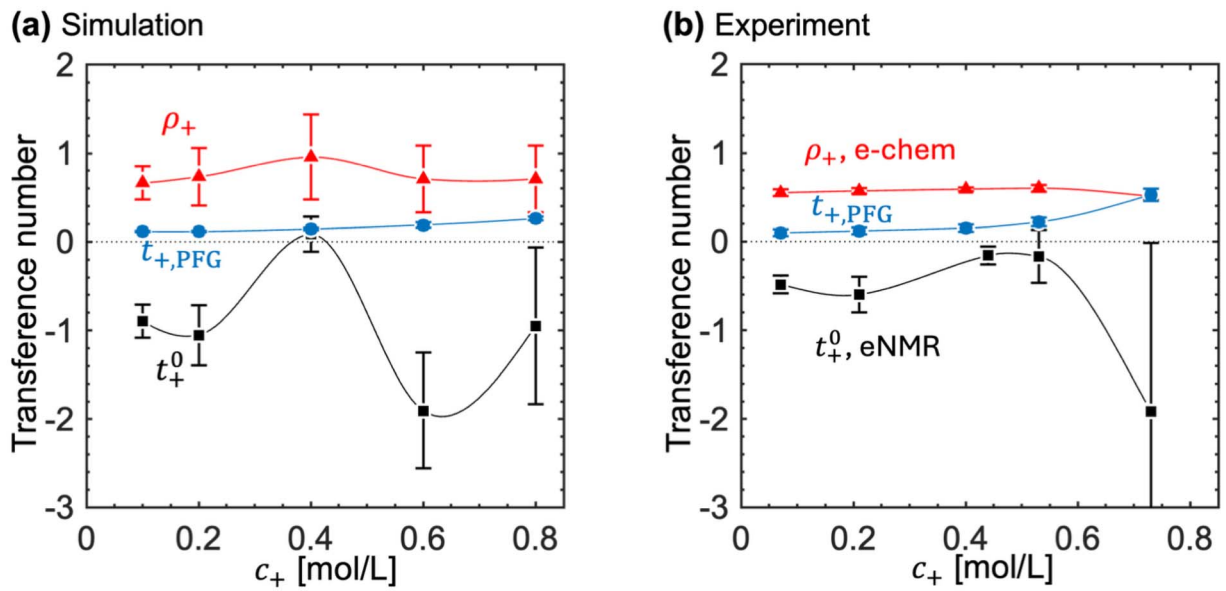

Fig. 3 Cation transference numbers from (a) simulation and (b) experiment as a function of Li^+ concentration. Three transference numbers are compared between simulation and experiment: the ideal transference number based on self-fusion coefficients $t_{+,\mathrm{PFG}} = \frac{D_+}{D_+ + 20D_-}$, the current fraction ρ_+, and the transference number in solvent reference frame t^0_+. The experimental transference numbers in (b) are reproduced from ref. 1.

concentrations, followed by a monotonic increase at higher concentrations. The agreement of $t_{+,\mathrm{PFG}}$ between simulation and experiment further verifies that the simulation can accurately reproduce the relative motion of ions and solvents as presented in Fig. 1.

Despite the low $t_{+,\mathrm{PFG}}$ values, the current fraction (ρ_+) exceeds 0.5 across all concentrations in both simulation and experiment. The result indicates that the transference of Li^+ under applied electric field is more efficient than predicted from self-diffusivities. It is attributed to ion association, consistent with the observation in previous studies of POSS-based anions.[12,23] The ion association can be quantitatively explained through correlated ion motion using the expression derived from eqn (4): $\rho_+ = (L^0_{++} - {L^0_{+-}}^2/L^0_{--})/(L^0_{++} - 2L^0_{+-} + L^0_{--})$, where the denominator is proportional to conductivity. The high ρ_+ values arise from two factors: (1) the dominance of anion correlated motion (L^0_{--}) over cation–anion correlations (L^0_{+-}) which reduces the subtraction term ${L^0_{+-}}^2/L^0_{--}$ in the numerator; (2) the relatively low conductivity from strong ionic correlations appeared in the denominator.

The rigorously defined transference number t^0_+ is negative or zero within error across all concentrations in both simulation and experiment. According to the expression in eqn (3), the negative t^0_+ is due to the weaker cation–cation correlations (L^0_{++}) compared to the cation–anion correlations (L^0_{+-}) as shown in Fig. 2. Throughout most of the concentration regime, t^0_+ values remain on the order of -1, indicating significantly unfavorable cation transference: a substantial fraction of cations migrate toward the positive electrode due to their association with the highly charged anions. It should also be noted that the concentration-dependence of t^0_+ surprisingly shows a peak near $c_+ = 0.4$ M. At the peak, t^0_+ in both simulation and experiment exhibit a value close to zero.

Solvation structure of lithium ions

To understand the correlated motion of ions and its impact on the low cation transference at the molecular level, we investigate the solvation structure of lithium ions. Fig. 4a depicts the evolution of the average number of solvent molecules and anions within a solvation shell of a lithium ion. The number of oxygen atoms from the anions (open symbols) is also shown to provide more details of lithium coordination. At all salt concentrations, more cyclic carbonates (EC) are present in the solvation shell than linear carbonates (DMC), in agreement with previous study of simple anions like PF_6^- in mixed carbonate electrolytes.[48–50] Even at the lowest concentration, each solvation shell is composed of roughly 0.8 POSS anions on average, which highlights significant cation–anion interactions for electrolytes containing POSS-based macroions. This is in stark contrast to the solvation structure of lithium ions in traditional univalent anions where anions are usually excluded from the solvation shell at low lithium concentrations.[48,49] As salt concentration increases, oxygens from POSS anion gradually displace solvent molecules in the solvation shell. The anions become the major component among the three coordinating species in the solvation shell in the $c_+ \geq 0.4$ M regime.

Given that each POSS anion provides plenty of oxygen coordination sites to lithium ions, it is instructive to quantify the fraction of lithium ions that bind to different number of anions. Fig. 4b shows that the fraction is maximized at one anion per lithium ion, indicating that 1 : 1 cation–anion binding is the most probable state. The cation can bind to 2 anions at most where the cation behaves as a bridge between two POSS macroanions. This overlap behavior of the anions only occurs in the concentration regime of $c_+ \geq 0.4$ M, which is consistent with the overlap behavior of anions suggested in previous work.[1] The overlap starts emerging at a critical salt concentration of $c_+ = 0.4$ M for the average distance between anions to equal their size of 4.4 nm. To further visualize the overlap of anions, the bottom of Fig. 4c presents the snapshots of anions and cations with increasing concentration. At $c_+ = 0.2$ M, the anions remain isolated from each other, with each of them binding to multiple lithium ions. At higher concentrations ($c_+ \geq 0.4$ M), the anions are bridged by lithium cations and form large aggregates.

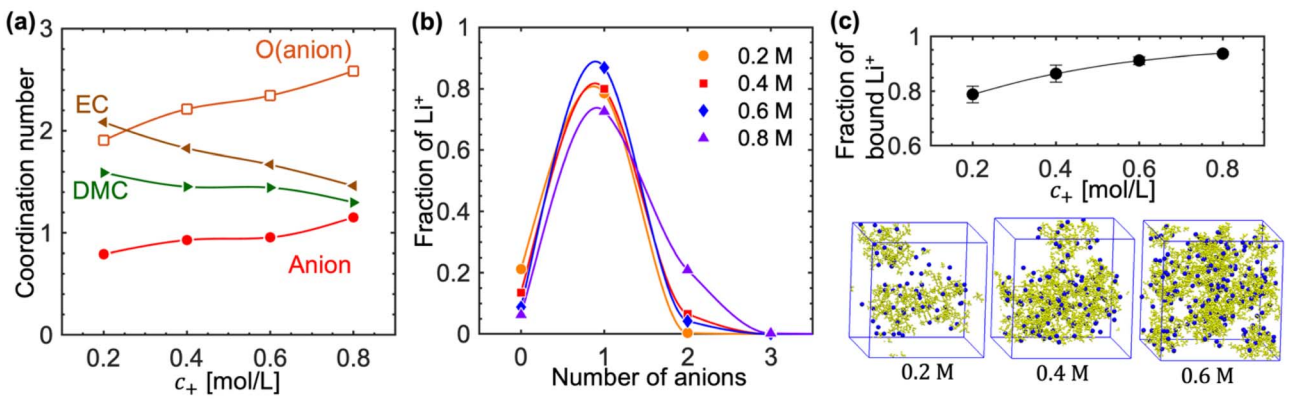

Fig. 4 Microscopic solvation structure of lithium ions. (a) Composition of the solvation shell of Li^+ as a function of salt concentration. The composition is quantified in terms of the average number of EC, DMC, and POSS anions (also oxygen from anions) in one solvation shell. (b) The fraction of lithium ions that bind to different number of POSS anions at different concentrations. (c) The ratio of anion-bound lithium ions to the total number of lithium ions as a function of salt concentration. The bottom shows the typical snapshots of cations and anions at three salt concentrations. The cations are shown in blue sphere, and anions are shown in yellow with ball-and-stick model.

Fig. 4b also shows that the fraction of non-bound lithium ions, *i.e.*, free cations only coordinated by solvent molecules but zero anions, decreases monotonically from 0.2 to 0.05. This corresponds to an increase in the fraction of bound lithium ions from 0.8 to 0.95 as shown in Fig. 4c. The fractions predicted by our MD simulations are in good agreement with the estimations based on eNMR species velocities in the previous work.[1] All together, these results demonstrate strong cation–anion interactions in the entire concentration regime which leads to highly correlated motion between cations and anions. It is the dominance of cation–anion correlations (L^r_{+-}) over the cation–cation correlations (L^r_{++}) that leads to the negative t^0_+ observed in Fig. 3.

Dynamics of lithium–anion association

In addition to the static properties of the solvation structure discussed above, the dynamics of cation–anion correlation is also important for understanding ion solvation and transport. We define residence time autocorrelation functions $C_i(t)$ to quantify the timescale of lithium–oxygen (either from POSS anion or solvent) coordination as:[50,51]

$$C_i(t) = \langle P_i(t)P_i(0)\rangle / \langle P_i(0)P_i(0)\rangle, \quad [i = \text{EC, DMC, or POSS anion}] \tag{6}$$

where $P_i(t)$ equals 1 when a lithium ion maintains continuous coordination with the same oxygen atom from species i from time 0 to t and equals 0 otherwise. The mean residence times (τ_i) are obtained by fitting $C_i(t)$ to stretched exponential functions. Fig. 5a shows that τ_{Anion} is significantly longer than τ_{EC} and τ_{DMC}. The difference is more pronounced at high salt concentrations, because each POSS anion has 20 TFSI^- units and several oxygen coordination sites on the side chains, which effectively enhances lithium–anion binding.

One surprising result is that t^0_+ exhibits a maximum in the vicinity of $c_+ = 0.4$ M. Both experiments and simulations show that t^0_+ becomes less negative and almost approaches 0 at such concentration. Some quantitative discrepancies remain. For instance, the simulated t^0_+ is slightly positive while the experimental value is slightly negative from 0.4 M to 0.5 M, which may originate from force field inaccuracies. A maximum in the cation transference usually implies an increase in the fraction of free cations. However, Fig. 4c shows that the fraction of free cations keeps decreasing with c_+. This inconsistency suggests that the maximum of t^0_+ observed in the POSS-based electrolytes cannot be attributed to the increase of free cations but other factors like ion correlations. To uncover the origin of the maximum t^0_+ in the vicinity of $c_+ = 0.4$ M, we decouple the cation correlated motion to two contributions, the self and distinct correlations, in the center-of-mass reference frame:[13,27]

$$L^m_{++} = L^{\text{self}}_{++} + L^{\text{distinct}}_{++}, \quad \text{with } L^{\text{self}}_{++} = \frac{D_+ c_+}{k_B T} \tag{7}$$

L^{self}_{++} is defined as the correlation of cations themselves (the summation with $\alpha = \beta$ in eqn (1)), while L^{distinct}_{++} is defined as the correlation between different cations (the summation with $\alpha \neq \beta$ in eqn (1)). Fig. 5b depicts their contributions relative to total cation correlations. L^m_{++} is dominated by the distinct term L^{distinct}_{++}, which contributes to more than 80% of the total cation correlation. On the other hand, the self-correlation term L^{self}_{++} only contributes to less than 20%. The large contribution of L^{distinct}_{++} arises from strong cation–anion pairing as illustrated in Fig. 4c, which promotes jointed motion of different cations bound to the same POSS anion.

More intriguingly, while the relative contributions of L^{self}_{++} and L^{distinct}_{++} remain constant in the salt concentration regime between 0.2 M and 0.4 M, Fig. 4b shows that the decrease of free cation fraction is mainly replaced by the fraction of cations bound to two anions. The fraction of cations bound to one anion remains constant in this concentration regime. Thus, the weak overlap of anions at 0.4 M mentioned earlier is accompanied by an additional fraction of cations acting as dynamic linkers. Because $L^{\text{self}}_{++}/L^m_{++}$ is constant as c_+ increases from 0.2 to 0.4 M, these lithium ions as linkers

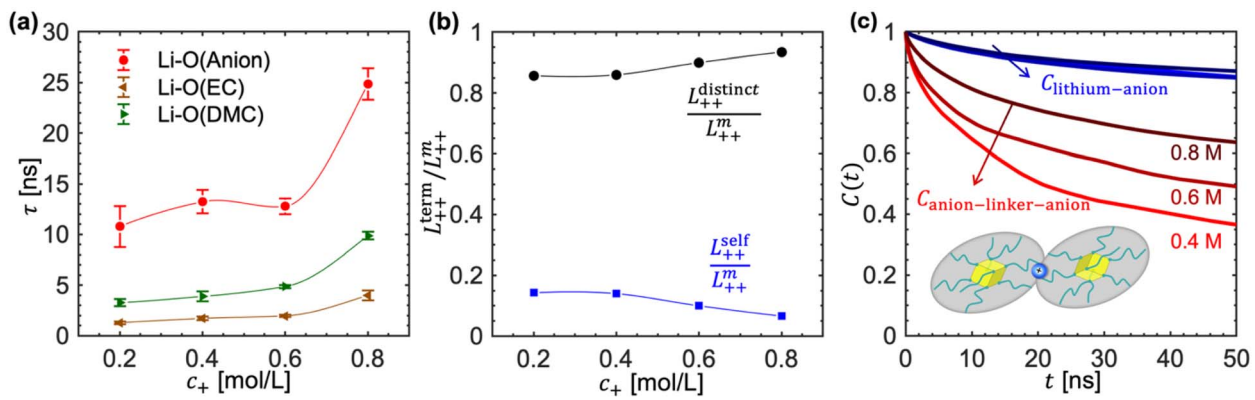

Fig. 5 Dynamics of ion association. (a) Mean residence times of Li–O(EC), Li–O(DMC), and Li–O(Anion) coordination as a function of salt concentration. (b) Decomposition of cation correlations into distinct (L^{distinct}_{++}) and self (L^{self}_{++}) correlation parts as a function of salt concentration. (c) Residence time autocorrelation functions for lithium as linker ($C_{\text{anion–linker–anion}}$) and for lithium bound to a single anion ($C_{\text{Li–anion}}$) from 0.4 M to 0.8 M. The lines for $C_{\text{Li–anion}}$ at the three concentrations cannot be clearly distinguished. The inset shows the schematic for lithium acting as linker to bridge two POSS anions.

resemble free cations in dynamics while providing insignificant contribution to correlated motion with anions.

To further elucidate the dynamic feature of lithium ions as linkers, we compare residence time autocorrelation functions for anion–linker–anion ($C_{\text{anion–linker–anion}}$) and lithium–single anion ($C_{\text{Li–anion}}$) associations. These time correlation functions are defined in a similar way as eqn (6), with the exception that a lithium is considered to associate with a POSS anion when POSS anion provides at least one oxygen for coordination. For $C_{\text{anion–linker–anion}}$, $P_i(t)$ defined in eqn (6) equals 1 when a linker is consistently connected to the same two anions from time 0 to t and equals 0 otherwise. Fig. 5c shows that, as salt concentration increases, $C_{\text{anion–linker–anion}}$ decays more slowly. On the other hand, the decay of $C_{\text{Li–anion}}$ only shows very weak concentration dependence. Furthermore, $C_{\text{anion–linker–anion}}$ decays much faster than $C_{\text{Li–anion}}$ and such difference is the most pronounced at $c_+ = 0.4$ M. The anion–linker–anion association has a very short lifetime at $c_+ = 0.4$ M, which leads to effective contribution to self-correlation of cations (L_{++}^{self}). Therefore, a relatively small L_{+-}^{m} in comparison with L_{++}^{m} at $c_+ = 0.4$ M explains the less negative value of t_+^0 at this concentration. It should be emphasized that the mechanistic interpretation of the fine feature in t_+^0 is based on relative dynamic correlations rather than absolute transport values. Therefore, the choice of current force field, which well captures cation transference, has a minimal impact of this finding.

Conclusion

To conclude, we have employed large-scale MD simulations to investigate ion transport in POSS-based multivalent lithium electrolytes. Using the Onsager transport framework, the simulation captures three cation transference numbers measured by recent experiments: the ideal transference number based on self-diffusion coefficients ($t_{+,\text{PFG}}$), the current fraction (ρ_+), and the transference number with respect to solvent velocity (t_+^0). The use of POSS anion yields $\rho_+ > 0.5$, whereas the true transference number t_+^0 is on the order of -1 across most concentration range. The Onsager transport coefficients reveal that the cation–cation, cation–anion, and anion–anion correlations are of comparable magnitudes in both solvent and center-of-mass reference frames, demonstrating strongly correlated motions of ions. The high ρ_+ arises due to the dominance of anion-correlated motion over cation–anion correlations and the small magnitude of the total conductivity. Analysis of the microscopic ion solvation environment indicates a strong cation–anion association in the entire concentration regime, which leads to negative t_+^0. Our MD simulations predict that t_+^0 approaches zero at a critical salt concentration of $c_+ = 0.4$ M, in agreement with experimental observations. A fraction of cations acts as dynamic linkers between weakly-overlapping anions. These linkers have very short lifetime and behave similarly as free cations in dynamics. Our work elucidates the molecular picture that bridges microscopic solvation structure, correlated motions between species, and the resulting macroscopic transference. The simulation results highlight the limitations of highly correlated ion motions in POSS electrolytes: while they enable high current fractions, they also lead to inefficient conduction and, crucially, unfavorable t_+^0.

Beyond diagnosing the limitations of POSS-based systems, our findings provide crucial design principles for electrolytes employing bulky/giant multivalent anions. The large negative t_+^0 primarily results from the strongly correlated cation–anion motion, which dominates over cation–cation correlations. Therefore, improved cation transference can be realized *via* strategies that effectively reduce cation–anion association. Such approaches may include: (1) modulating the charge distribution of multivalent anions, for instance, by increasing the steric hindrance between anions along a chain to prevent neighboring groups from binding the same Li^+; (2) optimizing the anion structure itself, such as by substituting $TFSI^-$ with the larger and more sterically hindered $BETI^-$ anion; (3) exploring solvents or additives (*e.g.*, triglyme) that strongly solvate cations, thereby alleviating the cation–anion coupling. These mechanistic insights extend beyond a single material system and constitutes a foundational framework for the rational design of next-generation electrolytes where mitigating detrimental cation–anion correlation is indispensable.

Conflicts of interest

There are no conflicts to declare.

Data availability

The data supporting this article have been included as part of the supplementary information (SI). Supplementary information: comparison of electrolyte density; standard force field corrections; obtaining transport coefficients; uncertainty estimation; conductivity from simulation; oxygen coordination of lithium; cluster approximation. See DOI: https://doi.org/10.1039/d5ta05739f.

Acknowledgements

This work was intellectually led by the Joint Center for Energy Storage Research (JCESR), an Energy Innovation Hub funded by the U.S. Department of Energy (DOE), Office of Science, Basic Energy Sciences (BES). Computations were conducted on the Savio Cluster at UC Berkeley and HPC-AI platform at HKUST(GZ).

References

1 S. Chakraborty, D. M. Halat, J. Im, D. T. Hickson, J. A. Reimer and N. P. Balsara, Lithium transference in electrolytes with star-shaped multivalent anions measured by electrophoretic NMR, *Phys. Chem. Chem. Phys.*, 2023, **25**(31), 21065–21073.
2 L. Onsager, Reciprocal relations in irreversible processes. II, *Phys. Rev.*, 1931, **38**(12), 2265.
3 J. Newman and N. P. Balsara, *Electrochemical Systems*, John Wiley & Sons, 2021.

4 Y. Choo, D. M. Halat, I. Villaluenga, K. Timachova and N. P. Balsara, Diffusion and migration in polymer electrolytes, *Prog. Polym. Sci.*, 2020, **103**, 101220.
5 K. W. Gao, C. Fang, D. M. Halat, A. Mistry, J. Newman and N. P. Balsara, The transference number, *Energy Environ. Mater.*, 2022, **5**(2), 366–369.
6 H. M. Goodwin, *The Fundamental Laws of Electrolytic Conduction: Memoirs by Faraday, Hittorf and F. Kohlrausch*, Harper & brothers, 1899.
7 M. Doyle, T. F. Fuller and J. Newman, The importance of the lithium ion transference number in lithium/polymer cells, *Electrochim. Acta*, 1994, **39**(13), 2073–2081.
8 L. Long, S. Wang, M. Xiao and Y. Meng, Polymer electrolytes for lithium polymer batteries, *J. Mater. Chem. A*, 2016, **4**(26), 10038–10069.
9 O. E. Geiculescu, R. Rajagopal, S. E. Creager, D. D. DesMarteau, X. Zhang and P. Fedkiw, Transport properties of solid polymer electrolytes prepared from oligomeric fluorosulfonimide lithium salts dissolved in high molecular weight poly (ethylene oxide), *J. Phys. Chem. B*, 2006, **110**(46), 23130–23135.
10 T. Trzeciak, L. Niedzicki, G. Groszek, P. Wieczorek, M. Marcinek and W. Wieczorek, New trivalent imidazole-derived salt for lithium-ion cell electrolyte, *J. Power Sources*, 2014, **252**, 229–234.
11 K. M. Diederichsen, K. D. Fong, R. C. Terrell, K. A. Persson and B. D. McCloskey, Investigation of solvent type and salt addition in high transference number nonaqueous polyelectrolyte solutions for lithium ion batteries, *Macromolecules*, 2018, **51**(21), 8761–8771.
12 T. K. L. Nguyen, T. N. Phan, F. Cousin, D. Devaux, S. Mehan, F. Ziarelli, S. Viel, D. Gigmes, P. Soudant and R. Bouchet, Polyhedral oligomeric silsesquioxane-based macroanions to level up the Li+ transport number of electrolytes for lithium batteries, *Chem. Mater.*, 2022, **34**(15), 6944–6957.
13 K. D. Fong, J. Self, B. D. McCloskey and K. A. Persson, Onsager transport coefficients and transference numbers in polyelectrolyte solutions and polymerized ionic liquids, *Macromolecules*, 2020, **53**(21), 9503–9512.
14 K. D. Fong, H. K. Bergstrom, B. D. McCloskey and K. K. Mandadapu, Transport phenomena in electrolyte solutions: Nonequilibrium thermodynamics and statistical mechanics, *AIChE J.*, 2020, **66**(12), e17091.
15 H. K. Bergstrom, K. D. Fong, D. M. Halat, C. A. Karouta, H. C. Celik, J. A. Reimer and B. D. McCloskey, Ion correlation and negative lithium transference in polyelectrolyte solutions, *Chem. Sci.*, 2023, **14**(24), 6546–6557.
16 A. R. Polu, H.-W. Rhee, M. J. K. Reddy, A. Shanmugharaj, S. H. Ryu and D. K. Kim, Effect of POSS-PEG hybrid nanoparticles on cycling performance of polyether-LiDFOB based solid polymer electrolytes for all solid-state Li-ion battery applications, *J. Ind. Eng. Chem.*, 2017, **45**, 68–77.
17 J. Ma, M. Zhang, C. Luo, M. Li, X. Guan, F. Chen and X. Ma, Polyethylene glycol functionalized polyhedral cage silsesquioxane as all solid-state polymer electrolyte for lithium metal batteries, *Solid State Ionics*, 2021, **363**, 115606.
18 I. Villaluenga, S. Inceoglu, X. Jiang, X. C. Chen, M. Chintapalli, D. R. Wang, D. Devaux and N. P. Balsara, Nanostructured single-ion-conducting hybrid electrolytes based on salty nanoparticles and block copolymers, *Macromolecules*, 2017, **50**(5), 1998–2005.
19 P. G. Bruce and C. A. Vincent, Steady state current flow in solid binary electrolyte cells, *J. Electroanal. Chem. Interfacial Electrochem.*, 1987, **225**(1–2), 1–17.
20 M. Watanabe, S. Nagano, K. Sanui and N. Ogata, Estimation of Li+ transport number in polymer electrolytes by the combination of complex impedance and potentiostatic polarization measurements, *Solid State Ionics*, 1988, **28**, 911–917.
21 P. R. Chinnam and S. L. Wunder, Polyoctahedral silsesquioxane-nanoparticle electrolytes for lithium batteries: POSS-lithium salts and POSS-PEGs, *Chem. Mater.*, 2011, **23**(23), 5111–5121.
22 P. R. Chinnam and S. L. Wunder, Self-assembled Janus-like multi-ionic lithium salts form nano-structured solid polymer electrolytes with high ionic conductivity and Li+ ion transference number, *J. Mater. Chem. A*, 2013, **1**(5), 1731–1739.
23 S. Chereddy, P. R. Chinnam, V. Chatare, S. Patrick diLuzio, M. P. Gobet, S. G. Greenbaum and S. L. Wunder, An alternative route to single ion conductivity using multi-ionic salts, *Mater. Horiz.*, 2018, **5**(3), 461–473.
24 M. D. Galluzzo, J. A. Maslyn, D. B. Shah and N. P. Balsara, Ohm's law for ion conduction in lithium and beyond-lithium battery electrolytes, *J. Chem. Phys.*, 2019, **151**, 020901.
25 D. M. Halat, A. Mistry, D. Hickson, V. Srinivasan, N. P. Balsara and J. A. Reimer, Transference Number of Electrolytes from the Velocity of a Single Species Measured by Electrophoretic NMR, *J. Electrochem. Soc.*, 2023, **170**(3), 030535.
26 D. R. Wheeler and J. Newman, Molecular dynamics simulations of multicomponent diffusion. 1. Equilibrium method, *J. Phys. Chem. B*, 2004, **108**(47), 18353–18361.
27 C. Fang, A. Mistry, V. Srinivasan, N. P. Balsara and R. Wang, Elucidating the molecular origins of the transference number in battery electrolytes using computer simulations, *JACS Au*, 2023, **3**(2), 306–315.
28 E. R. Chan, A. Striolo, C. McCabe, P. T. Cummings and S. C. Glotzer, Coarse-grained force field for simulating polymer-tethered silsesquioxane self-assembly in solution, *J. Chem. Phys.*, 2007, **127**, 114102.
29 W. L. Jorgensen, D. S. Maxwell and J. Tirado-Rives, Development and testing of the OPLS all-atom force field on conformational energetics and properties of organic liquids, *J. Am. Chem. Soc.*, 1996, **118**(45), 11225–11236.
30 L. S. Dodda, I. Cabeza de Vaca, J. Tirado-Rives and W. L. Jorgensen, LigParGen web server: an automatic OPLS-AA parameter generator for organic ligands, *Nucleic Acids Res.*, 2017, **45**(W1), W331–W336.
31 C. I. Bayly, P. Cieplak, W. Cornell and P. A. Kollman, A well-behaved electrostatic potential based method using charge

restraints for deriving atomic charges: the RESP model, *J. Phys. Chem.*, 1993, **97**(40), 10269–10280.
32 J. Zeng, L. Duan, J. Z. Zhang and Y. Mei, A numerically stable restrained electrostatic potential charge fitting method, *J. Comput. Chem.*, 2013, **34**(10), 847–853.
33 M. Frisch, G. Trucks, H. Schlegel, G. Scuseria, M. Robb, J. Cheeseman, G. Scalmani, V. Barone, G. Petersson and H. Nakatsuji, *Gaussian 16, Revision A. 03*, Gaussian Inc., Wallingford CT, 2016.
34 J. Wang, R. M. Wolf, J. W. Caldwell, P. A. Kollman and D. A. Case, Development and testing of a general amber force field, *J. Comput. Chem.*, 2004, **25**(9), 1157–1174.
35 M. J. Abraham, T. Murtola, R. Schulz, S. Páll, J. C. Smith, B. Hess and E. Lindahl, GROMACS: High performance molecular simulations through multi-level parallelism from laptops to supercomputers, *SoftwareX*, 2015, **1**, 19–25.
36 G. Bussi, D. Donadio and M. Parrinello, Canonical sampling through velocity rescaling, *J. Chem. Phys.*, 2007, **126**, 014101.
37 H. J. Berendsen, J. V. Postma, W. F. Van Gunsteren, A. DiNola and J. R. Haak, Molecular dynamics with coupling to an external bath, *J. Chem. Phys.*, 1984, **81**(8), 3684–3690.
38 B. Hess, H. Bekker, H. J. Berendsen and J. G. Fraaije, LINCS: A linear constraint solver for molecular simulations, *J. Comput. Chem.*, 1997, **18**(12), 1463–1472.
39 T. Darden, D. York and L. Pedersen, Particle mesh Ewald: An N log (N) method for Ewald sums in large systems, *J. Chem. Phys.*, 1993, **98**, 10089.
40 Y. Shao, H. Gudla, D. Brandell and C. Zhang, Transference number in polymer electrolytes: mind the reference-frame gap, *J. Am. Chem. Soc.*, 2022, **144**(17), 7583–7587.
41 A. Mistry, Z. Yu, B. L. Peters, C. Fang, R. Wang, L. A. Curtiss, N. P. Balsara, L. Cheng and V. Srinivasan, Toward bottom-up understanding of transport in concentrated battery electrolytes, *ACS Cent. Sci.*, 2022, **8**(7), 880–890.
42 Y. Shao, H. Gudla, J. Mindemark, D. Brandell and C. Zhang, Ion transport in polymer electrolytes: Building new bridges between experiment and molecular simulation, *Acc. Chem. Res.*, 2024, **57**(8), 1123–1134.
43 C. Fang, X. Yu, S. Chakraborty, N. P. Balsara and R. Wang, Molecular origin of high cation transference in mixtures of poly (pentyl malonate) and lithium salt, *ACS Macro Lett.*, 2023, **12**(5), 612–618.
44 N. P. Balsara and J. Newman, Relationship between steady-state current in symmetric cells and transference number of electrolytes comprising univalent and multivalent ions, *J. Electrochem. Soc.*, 2015, **162**(14), A2720.
45 C. Schröder, Comparing reduced partial charge models with polarizable simulations of ionic liquids, *Phys. Chem. Chem. Phys.*, 2012, **14**(9), 3089–3102.
46 M. I. Chaudhari, J. R. Nair, L. R. Pratt, F. A. Soto, P. B. Balbuena and S. B. Rempe, Scaling atomic partial charges of carbonate solvents for lithium ion solvation and diffusion, *J. Chem. Theor. Comput.*, 2016, **12**(12), 5709–5718.
47 Z. Li, L. A. Robertson, I. A. Shkrob, K. C. Smith, L. Cheng, L. Zhang and J. S. Moore, Realistic Ion Dynamics through Charge Renormalization in Nonaqueous Electrolytes, *J. Phys. Chem. B*, 2020, **124**(15), 3214–3220.
48 X. Bogle, R. Vazquez, S. Greenbaum, A. V. W. Cresce and K. Xu, Understanding Li+–solvent interaction in nonaqueous carbonate electrolytes with 17O NMR, *J. Phys. Chem. Lett.*, 2013, **4**(10), 1664–1668.
49 C.-C. Su, M. He, R. Amine, T. Rojas, L. Cheng, A. T. Ngo and K. Amine, Solvating power series of electrolyte solvents for lithium batteries, *Energy Environ. Sci.*, 2019, **12**(4), 1249–1254.
50 C. Fang, D. M. Halat, A. Mistry, J. A. Reimer, N. P. Balsara and R. Wang, Quantifying selective solvent transport under an electric field in mixed-solvent electrolytes, *Chem. Sci.*, 2023, **14**(20), 5332–5339.
51 O. Borodin and G. Smith, Li+ transport mechanism in oligo (ethylene oxide) s compared to carbonates, *J. Solut. Chem.*, 2007, **36**, 803–813.

